SUPPLEMENTAL MATERIALS

Assessment of the Radiation Effects of Cardiac CT Angiography Using Protein and Genetic Biomarkers

Patricia K. Nguyen, MD[1,2,3]*, Won Hee Lee, PhD[1,3]*, Yong Fuga Li, PhD[4]*, Wan Xing Hong, BS[1,3], Shijun Hu, PhD[1,3], Charles Chan, PhD[5], Grace Liang, BS,[1] Ivy Nguyen,[1] Sang-Ging Ong, PhD[1,2], Jared Churko, PhD[1,3], Jia Wang, PhD[6], Russ B. Altman, PhD[4], Dominik Fleishmann, MD[1,7], Joseph C. Wu, MD, PhD[1,3,7]

[1]Stanford Cardiovascular Institute; [2]Veterans Administration Palo Alto; [3]Department of Medicine, Division of Cardiology; [4]Department of Genetics; [5]Department of Surgery; [6]Environmental Health and Safety; [7]Department of Radiology, Stanford University School of Medicine, Stanford, CA 94305

*Contributed equally

SUPPLEMENTAL METHODS

Patients and diagnostic imaging studies. Patients underwent cardiac CTA using 64-channel CT scanners (Sensation Dual Source, Siemens Medical Solutions, Forchheim, Germany or Discovery 750HD, GE, Milwaukee, Wisconsin) after the intravenous administration of iodinated contrast iopamidol (Isovue-370, Bracco Diagnostics, Princeton, NJ) or iohexol (Omnipaque-350, GE Healthcare, Princeton, NJ) at 4-5 ml/sec. Demographic and clinical information was obtained from the electronic medical record. Patients with a recent history of exposure to radiation producing imaging tests (<1 month) and a recent diagnosis of cancer were excluded. Fifteen adult patients who underwent echocardiography using a VIVID7 ultrasound machine (GE) were also recruited to serve as a negative control group for the study.

Estimation of radiation dose. One blinded investigator (JiW) entered the radiation exposure factors into the ImPACT spreadsheet, which estimates the organ-specific radiation dose using NRPB-SR250 Monte Carlo data sets matched to the computed tomographic system. These radiation factors included the following: 1) information on the scanning parameters (manufacturer, scanner model, kV, and scan region), 2) Monte Carlo data set, 3) scan range (start position and end position), 4) patient sex, and 5) acquisition parameters (mA, rotation time, mAs/rotation, collimation, slice width, pitch, relative CTDI, CTDI (air), CTDI (air), CTDI (soft tissue) and ${}_{n}CTDI_{w}$.). Organ specific blood volumes were estimated from a previous report (1). The total blood volume dose was obtained by summing organ-specific doses weighted according to the blood content in each organ. Dose length product (DLP) and computed tomographic dose index (CTDI) were obtained from dose reports generated at the end of each cardiac CTA study.

Sample collection for *in vivo* studies. Whole blood was collected by venipuncture into vacutainer tubes containing EDTA. Blood was collected by venipuncture prior to (i.e., baseline) and after the

cardiac CTA and placed immediately on ice to arrest DNA repair. For the evaluation of DNA damage by flow cytometry, blood was collected at baseline and 30 minutes after exposure in all patients. In a subset of patients (n=25), immunohistochemistry was used to evaluate the kinetics of cellular response to radiation and measure the amount of apoptosis at baseline and at the following serial time points post-irradiation: a) 5, 15, 30, 60, and 120 minutes; b) 6, 24, and 48 hours; c) 1 week; and d) 1 month. Whole genomic profiling was performed at baseline and 24 hours post-radiation exposure in a subset of patients (n=3) to help determine which genes to analyze by single cell polymerase chain reaction (PCR) in the entire cohort. Single cell PCR was performed at baseline and at 24 hours post-irradiation in all patients to determine the expression profiles of these select genes (**Supplemental Table 1**). In a subset of patients (n=51), serial PCR was performed at baseline and the following time points post-irradiation to determine the time course for gene expression changes: a) 2, 6, 24, and 48 hours; b) 1 month; and c) 1 week.

Biomarkers for DNA damage. Analyses of protein biomarkers of DNA damage and apoptosis by flow cytometry and immunohistochemistry were performed using standard protocols. DNA damage biomarkers included phosphorylated H2AX, ATM, and p53. Programmed cell death biomarkers included annexin and DAPI by flow cytometry and BAX and DAPI by immunohistochemistry. Specifically, T cell isolation was performed using the RosetteSep® Human T Cell Enrichment Cocktail (StemCell Technologies), according the manufacturer's protocol. Briefly, after incubation of whole blood with the T Cell Enrichment Cocktail, T cells were isolated from the buffy coat using density gradient centrifugation on 1.077 g/ml Ficoll-Paque^{TM} Plus (Amersham/GE Healthcare). Total and phosphorylated forms of H2AX were determined using FlowCellect™ Dual Detection kits (Millipore, Billerica, MD), according to the

manufacturer's instructions. Briefly, T cells were fixed in fixation buffer for 20 minutes at room temperature. After permeabilizing cells on ice for ten minutes, cells were incubated with anti-phospho H2AX-PerCP (Millipore, Billerica, MD), and anti-H2AX-FITC (Millipore, Billerica, MD) for 30 minutes in the dark at room temperature. In order to detect phosphorylation of ATM and p53, cells were labeled with either pATM-PE (Millipore, Billerica, MD) or pp53-FITC (Cell Signaling Technology, Danvers, MD) in the dark on ice for 60 minutes. Finally, cells were re-suspended in fluorescence-activated cell sorting (FACS) buffers (DPBS with 2% FBS and 2 mM EDTA) and analyzed using a FACScan (BD Biosciences, Franklin Lakes, NJ). For each antigen analyzed, the percentage of positive cells was determined in relationship to the following isotype controls: mouse IgG-PerCP (Abcam, Cambridge, MA) rabbit IgG-FITC (Abcam, Cambridge, MA), mouse IgG-PE, and mouse IgG-FITC (Millipore, Billerica, MD). Ten thousand events were analyzed by FACS.

Analysis of programmed cell death. For analysis of apoptosis, whole blood was treated with ACK Lysis Buffer (Life Technologies, Carlsbad, CA) to remove red blood cells and purify white blood cells. The remaining white blood cells then underwent Fc block (BD Biosciences, Franklin Lakes, NJ) for 10 minutes on ice to prevent nonspecific antibody binding before being labeled with CD3-APC antibody (BioLegend, San Diego, CA). Staining with CD3-APC was carried out in the dark on ice with an incubation period of 15 minutes. Following staining, excess antibodies were removed through a wash with Annexin Binding Buffer. Cells were then stained with Annexin V-PerCP Cy5.5 (BD-BioSciences) and DAPI (Life Technologies) in 100 ul of Annexin Binding Buffer. Staining was carried out in the dark at room temperature for 15 minutes. Finally, cells were re-suspended in FACs buffers (DPBS with 2% FBS and 2 mM EDTA) and analyzed using a

FACScan (BD Biosciences, Franklin Lakes, NJ). One hundred thousand events were collected. Data for markers of DNA damage and apoptosis were analyzed using FlowJo software (TreeStar).

Immunocytochemistry. Isolated T-cells (~1.6×10^5 cells/150µl per slide) were spun onto Superfrost/Plus microscope slides (Fisher Scientific, Pittsburgh, PA) using the Cytospin 4 (Thermo Scientific; Waltham, MA) at 500 rpm for 5 minutes at low acceleration. Cells were fixed in 4% paraformaldehyde for 15 minutes at room temperature. After rinsing with phosphate buffered saline (PBS), cells were blocked, and permeabilized in 5% bovine serum albumin (BSA) and 0.2% Triton X-100 for an hour at room temperature, followed by incubation with primary antibodies, such as mouse anti-γH2AX (Ser139) monoclonal antibody (Millipore, Billerica, MA), mouse anti-phospho-ATM (Ser1981) monoclonal antibody (Millipore), goat anti-53BP1 polyclonal antibody (R&D System, Minneapolis, MN), rabbit anti-BAX monoclonal antibody (Cell Signaling), and rat anti-CD3 monoclonal antibody (AbD Serotec, Düsseldorf, Germany) diluted in antibody diluent buffer (IHC World, Woodstock, MD) overnight at 4 °C. Cells were then washed with 0.2% Tween-20 in PBS. After additional rinsing with PBS, cells were incubated in the dark for 1 hour with a secondary antibody, either goat-anti-mouse IgG conjugated with Alexa Fluor 488 or goat-anti-rat IgG conjugated with Alexa Fluor 594. The slides were washed and nuclei were counterstained with DAPI. γH2AX (phosphorylated at serine 139) foci/lymphocyte was examined using a fluorescence microscope with 40x magnification. One hundred cells were counted by two blinded observers.

Whole genome profiling (RNA sequencing). Total RNA was isolated from T-lymphocytes using miRNeasy kit (Qiagen, Valencia, CA) following the manufacture's protocol, and DNAse treatment

was performed using RNase-free DNase kit (Qiagen). One hundred ng of total RNA was converted to cDNA and amplified using NuGen V2 RNA-seq kit (NuGen, San Carlos, CA). cDNA was fragmented to an average of 300 bps using the Covaris S2, and Illumina sequencing adapters were ligated to 500 ng of cDNA using NEBNext® mRNA Library Prep Reagent Set (New England Biolabs, Ipswich, MA). PCR was performed on the adapter-ligated cDNA using the following conditions (denaturation 98 °C for 30 seconds, following 12 cycles of denaturation 98 °C for 10 seconds, annealing 65 °C for 30 seconds and extension 72 °C for 30 seconds, ending with an extension at 72 °C for 5 minutes). Libraries were submitted to the Stanford Stem Cell Institute Genome Center for sequencing using Illumina's HiSeq2000 platform using paired in reads at an average length of 100 bps (2x100). Reads were mapped with Tophat 2.0.8b using the hg19 reference annotation. Cuffcompare and Cuffdiff were then used to determine, which gene levels were significantly different ($q<0.05$).

Single cell real time PCR. Following irradiation and cell culture, the blood was diluted 1:1 with Dulbecco's phosphate buffered saline (DPBS). After peripheral blood mononuclear cell (PBMC) isolation and purification using density gradient centrifugation on 1.077 g/ml Ficoll-Paque^{TM} Plus (Amersham/GE Healthcare), FACS was performed to isolate T cells. Briefly, cells were pre-incubated with 20 µl of FcR-blocking reagent (Miltenyi Biotec, Auburn, CA), stained with 5 µl of fluorochrome-labeled antibodies (anti-CD3-APC, anti-CD20-PE-Cy7, and anti-CD56-FITC), and incubated in 100 µl of FACS buffer (PBS containing 2% FBS, 2 mM EDTA) on ice for 30 min. To check cell viability, 7-Amino-Actinomycin D (7-AAD) was added to PBMC cell suspension just prior to sorting using a FACS Aria (BD Biosciences, Mississauga, Canada) into 96-well 0.2 ml PCR plates containing buffers and enzymes for reverse transcription according to the

manufacturer's instructions (Fluidigm, South San Francisco, CA). Each well contained reverse transcription-specific target amplification (RT-STA) master mix including 2 × CellsDirect reaction mix (CellsDirect One-Step qRT-PCR kit), SUPERase-In (Applied Biosystems) for prevention of RNA degradation by RNases, a pool of all Taqman primers defining DNA damage responses (Applied Biosystems; **Supplemental Table 1**), and a mixture of different enzymes, SuperScript II Reverse Transcriptase and Platinum Taq DNA polymerase (Invitrogen, Grand Island, NY), for the RT-STA reaction. Reverse transcription and specific amplification of individual genes were performed using the following protocol: 50 °C for 15 min, 70 °C for 2 min, 95 °C for 15 sec, and 60 °C for 4 min, repeated 18 times. Quantitative real-time PCR was then conducted on a Fluidigm 48×48 Dynamic Array microfluidic chip by partitioning the samples into 48 microfluidic chambers, running in a BioMark HD reader, analyzing with the Fluidigm Real-time PCR analysis software. Results are shown as threshold cycles (C_T), which measure target transcript abundance in the samples. All reactions were performed in duplicates or triplicates.

Whole blood irradiation model for in vitro studies. Whole blood was collected by venipuncture into vacutainer tubes containing EDTA. For the evaluation of proteomic changes in vitro, 20 ml of blood (4 ml per each irradiation dose) was collected from individual donors with blood type O and placed immediately on ice prior to irradiation. For evaluation of gene expression *in vitro*, a total of 45 ml of blood was collected from eight health volunteers with blood type O positive and divided into five aliquots of blood for each radiation dose (i.e., 0, 12.5, 25, 50, 5000 mGy). Control samples received sham-irradiation. Immediately after irradiation, blood samples were incubated at 37°C in 5% CO_2/95% air until the appropriate time point for analysis. For incubation times longer than 30 minutes, blood samples were diluted 1:1 with RPMI 1640 medium (Mediatech Inc.)

supplemented with 10% heat-inactivated fetal bovine serum to maintain cell viability. Evaluation of protein and genetic biomarkers were performed within two minutes of the appropriate time point and repeated three times.

SUPPLEMENTAL STATISTICAL ANALYSIS

Evaluation of normality and transformation of variables. The skewness and kurtosis test was used to determine whether data were normally distributed. If data were not normally distributed, data were transformed as follows: 1) square root transformation for maximum percent change in protein phosphorylation, 2) inverse square root transformation for maximum percent and fold apoptosis, and 3) rank transformation for gene expression by single cell PCR.

Evaluation of whole genome data sets. Only transcripts uniquely mapped to genes were retained. The read-counts for multiple transcripts mapped to the same genes were aggregately by summation at linear-scale. Gene level reads-counts were log2 transformed with pseudo-count of 1. Only protein coding genes are included, and the expression of genes were quantile normalized for subsequent analysis.(2)

To extract the radiation response, we use the following linear model for observed gene expression level x_{gij} for gene g, individual i, and radiation status j:

$$x_{gij} \sim \mu_g + b_{gi} + r_g + \varepsilon_{gij}$$

where μ_g is the baseline gene expression of gene g (a protein coding gene), b_{gi} is the individual effect of gene g in individual i (patient 6, 7, or 8), r_{gj} is the radiation effect on gene g at radiation

status j (before or 24h after radiation), and ε_{gij} is a measurement noise. For individuals 6, 7, and 8, the radiation doses are 48.8, 21.3, and 36.0 milliSieverts (mSv), respectively. Incorporating the dose information into the linear model did not lead to significant change in the results, hence the simpler model without dose is used. To identify functionally important transcription factors, gene function classes, and pathways responding to low-dose radiation in human blood, we performed enrichment analyses of the top perturbed genes against three types of genes annotations (gene sets), including the transcription factor target genes (TFTG) database we compiled in-house from ENCODE and other ChIP-seq as well as low throughput experiment (3), the Gene Ontology (GO) Biological Processes (4), and canonical pathways from Reactome (5), KEGG (6), and BioCarta (7), and pharmacogenomics pathways from PharmGKB (8).

Gene expression changes following radiation (i.e., the radiation effect r_{gj} estimated in the model described above) were sorted and discretized into 3 categories: top 5% of genes with increased expression following radiation, bottom 5% of genes with decreased expression following radiation, and middle 90% with small or no changes. Associations of the discretized gene expression with the gene sets described above were then performed on the 3 by 2 table based on the multivariate hypergeometric distribution, which gives an extension of standard Fisher's exact test (9). In addition, linear models and the Wald test were used to evaluate the average expression changes of genes annotated with a functional category compared with other genes, by treating genes' radiation effect r_{gj} as a response variable, and gene annotation as a binary explanatory variable.

During an initial analysis, we discovered that many of the significantly perturbed transcription factors, gene function classes, and pathways are enriched with histone genes. These histone genes form spatial clusters within the human genome, and histone genes within the same

family share high sequence similarities; namely, H2B family genes HIST1H2BE and HIST1H2BM are both at chromosome band 6p22.1 and they share 89% sequence identity at the nucleotide level. This results in possible cross-contamination in the quantification of these close homolog genes, as a result of same reads mapped to multiple histone genes. Although RNA-seq is believed to resolve paralogs better than microarray (10), we removed 83 histone genes from the functional enrichment analysis in order to achieve a conservative result. To correct for multiple testing, we convert the p-values obtained from each of the three type of enrichment analysis to q-values and a q-value cutoff of 0.05 is used unless otherwise specified. To correct for multiple testing, we convert the p-values obtained from each of the three type of enrichment analysis to q-values, and a q-value cutoff of 0.1 is used in this study unless otherwise specified (11).

Analysis of single cell PCR results. Gene expression data were analyzed using the equation $2^{-\Delta\Delta CT}$, where $\Delta\Delta C_T$ = [C_T of target gene - C_T of housekeeping gene] $_{\text{treated group}}$ – [C_T of target gene - C_T of housekeeping gene] $_{\text{untreated control group}}$. For the treated samples, evaluation of $2^{-\Delta\Delta CT}$ indicates the fold change in gene expression, normalized by a housekeeping gene (18S), and relative to the untreated control. The relative expression levels of target genes identified by single cell PCR were calculated using the ΔΔCt method after normalizing to 18S housekeeping gene. Differences in gene expression over time were compared using repeated measures of ANOVA after rank transformation, followed by post-hoc Student's t test to compare maximum fold change in gene expression.

Multivariate logistic regression modeling. In the absence of established cutoffs, we categorized participants a priori using the following criteria for descriptive purposes: 1) the presence of

programmed cell death was defined as having ≥2-fold increase in expression of protein biomarkers of apoptotic cells; 2) the presence of gene activation was defined as having ≥2-fold change in genes involved in DNA repair and apoptosis. The presence of DNA damage was defined as ≥2% increase in any of the protein markers of DNA damage, based on previous findings that the median change in phosphorylation in a negative control group undergoing echocardiography was less than 1% (data are not shown). We propose the following three null hypotheses: cardiac CTA radiation dose is *not* associated with 1) DNA damage, 2) gene activation, or 3) cellular apoptosis. To evaluate these hypotheses, we used multivariate logistic regressions to model the binary outcomes of the presence or absence of DNA damage, gene activation, and apoptosis with the 8 covariates (excluding total effective dose) detailed in **Table 1**. For testing the first hypothesis, we used data from patients undergoing proteomic analysis. For testing the second and third hypothesis, we only used data from the subset of patients who underwent genomic biomarker and programmed cell death analyses, respectively. Although it is well accepted that DNA damage is directly proportional to dosage at radiation doses ≥100 mSv, whether this relationship exists at lower doses is still under debate. We also tested whether DNA damage was a better predictor than dose for gene activation and apoptosis by replacing dose with DNA damage as an additional continuous covariate in the logistic regression as the two cannot be modeled together because the effects of dose are likely captured by DNA damage. Other potential confounders (i.e., mean iodine content) were not included in the logistic regression model.

Sample size and power. Based on a difference of 1.6% in phosphorylation of H2AX after 12.0 mSv of radiation *in vitro*, we have more than 80% power, assuming a standard deviation of 0.2 and a sample size of 57 participants.

SUPPLEMENTAL RESULTS

Clinical and scan parameters. The subjects were predominantly middle aged (median: 67 years), slightly overweight (mean BMI: 26.5 kg/m^2), Caucasian (80.1%), men (78.9%), who were nonsmokers (78.9%), and did not have a prior history of cancer (77.2%) **(Table 1).** The median effective dose to the body was 36.9 mSv (26.1 – 67.1 mSv), which is equivalent to 1,845 chest X-rays. The median DLP was 1535.3 mGy·cm (969.7 – 2674.0 mGy·cm). The median radiation exposure to the blood was 29.8 mSv [18.8 – 48.8 mSv]. Because doses to the blood ranged from a minimum of 2.0 mSv to a maximum of 90.8 mSv in our cohort, we were able to capture a wide range of dose effects.

Cardiac CTA was performed for the following indications: 1) evaluation of the aorta (n=30), 2) assessment of coronaries to exclude obstructive coronary artery disease (n=23), 3) surgical planning for transcatheter valve replacement (n=18), and 4) left atrial mapping prior to atrial fibrillation ablation (n=3) (**Supplemental Table 2**). Cardiac CTA was performed using the following scan parameters: 1) tube voltage of 120 kV, 2) rotation time of 0.26 – 0.5 seconds, 3) spiral pitch of 0.2 – 0.8, and 4) collimation for gated helical scans of 64 mm x 0.6 mm. Effective amperages were 100 mAs for the chest scans and 160 mAs for the abdomen and pelvis scans (i.e., Note patients that had evaluation of the entire aorta and its branches had scans of their chest, abdomen, and pelvis). Both retrospective gating with dose modulation and prospective gating were used. Fifteen patients were excluded because they declined to participate (n=5), they had recent (< 1 month) exposure to x-ray imaging (n=3), they did not complete the cardiac CTA (n=2), or their lymphocytes could not be isolated due to technical difficulties (n=5) (**Figure 1**).

Whole genome profiling. Three patients were carefully chosen to represent a wide range of doses of radiation exposure and shared similar characteristics to the study cohort (**Supplemental Table 4**). From a Euclidean distance-based hierarchical clustering analysis of the samples, we observed that before-after radiation pairs for the same individuals clustered together, suggesting that biological variation among individuals was responsible for most of the gene expression variations among the samples, which is not unexpected given the radiation dose and diversity (gender and age, etc.) in participating patients (note – sample size should not matter much in this analysis) (**Supplemental Figure 4A**). In fact, the two patients (6 and 7) found to be more similar are both females, and they both have weaker average gene expression changes than patient 8. The average absolute log2 fold changes are 0.23 and 0.24 for female patients 6 and 7, and 0.41 for male patient 8 (p-values from F-test comparing patient 7/6, 8/6, 8/7 are 0.058, 3.2×10^{-1039}, and 1.4×10^{-994}, respectively). Based on an analysis of variance (ANOVA) using an additive model, 10.0% of the gene expression variations came from radiation response, while 73.2% of the variations come from biological variations among individuals, with the remaining 16.8% from technical variations (noise).

When we perform single gene level significance tests for the before and after radiation comparisons, we identified 613 protein coding genes at p-value cutoff 0.05 using a linear model with additive effects of individuals variations and radiation responses (see **Supplemental Methods**), but none of these genes passed q-value cutoff 0.05. This is due to a combination of weak signal and relatively small sample size. Despite this, we observe a significant signal when we combine all genes together using Fisher's method that combines the p-values from all genes (degree of freedom 29830, $\chi^2 = 31364.4$, $p=3.2 \times 10^{-10}$). In addition, we find that the global patterns of differential gene expressions from the three individuals are significantly and positively

correlated. The p-values of Spearman's rank correlation between patients 6 and 7, patients 6 and 8, and patients 7 and 8 are 0.3, $1x10^{-9}$, and $1x10^{-71}$, respectively, suggesting that there are detectable signals at the whole transcriptome level. Notice that the two patients that have higher doses (patients 7 and 8 with 48.8 mSv and 36.0 mSv, respectively) have highly correlated transcriptome responses, although the two female patients 6 and 7 have similar magnitude of responses, which is lower than that of male patient 8.

Interestingly, when we examined the known functions of these transcription factors, we found that 39 transcription factors were significantly altered after exposure to radiation exposure from cardiac CTA, and these include 3 transcription factors involved in apoptosis (NFκB1, E2F1, and TP53), 8 involved in cell cycle regulation (GFI1, CCNT2, TAF1, E2F1, MYC, TP53, GFI1B, and SMC3), 1 involved in DNA repair (TP53), and 4 involved in stress response (EPAS1, NFκB1, SREBF1, and TP53) (**Supplemental Table 8**). NFκB1 is a transcriptional activator and a negative regulator of apoptosis (12). We found that the target genes of NFκB1 were down-regulated on average (**Figure 4** and **Supplemental Table 5**), suggesting that NFκB1 activity was suppressed 24 hours after cardiac CTA exposure, and hence apoptosis was up-regulated. EPAS1 (HIF2A) is an important hypoxia and radiation response gene. Inhibition of EPAS1 is known to promote p53 activity and radiation response in cancer cells (13). Normally, hypoxia induces EPAS1 activity and subsequently activates down stream genes. We found that the target genes of EPAS1 are down-regulated after cardiac CTA (**Figure 4**), suggesting that EPAS1 activity was suppressed by the radiation, consistent with the increased levels of programmed cell death.

One interesting trend we observed was that majority of the transcription factors showed decreased target gene expression levels following radiation (**Figure 4** and **Supplemental Table 8**), while the expression levels of transcription factors themselves (rather than their target genes)

were also decreased overall when we aggregated the expression of the top 39 significant transcription factors with q-values below 0.1 (*P=0.012 by sign test, and *P=0.022 by Student's t-test, **Figure 4**).

The associations from signaling/metabolic pathways were consistent with the transcription factors identified. For example, the HIF1A pathway was significant (Wald t test P= $1.2x10^{-5}$, Fisher's exact test *P=$1.4x10^{-3}$), while transcription factors EPSA1 and HIF1A were also significant (**Figure 4** and **Supplemental Table 5**); similarly, both the NFAT pathway and transcription factor NFATC1 were significant. Interestingly, the metabolic pathway responsible for the pentose phosphate metabolic pathway was found to be significantly down-regulated 24 hours after cardiac CTA (Wald t test P=$2.3x10^{-5}$, Fisher's exact test P=$1.0x10^{-3}$). The pentose phosphate pathway plays an important role in counteracting oxidation stress (14), and protects cells against radiation-induced cell death (15). The reduced expression of enzymes of pentose phosphate pathway was consistent with increased apoptosis after cardiac CTA.

Weaker signals were observed from the GO biological processes (**Supplemental Table 6**). In fact, none of the top GO annotations detected by Fisher's exact test are directly related to cellular apoptosis, cell cycle, or DNA repair. However, by using Wald test of the average expression changes of genes, we identified three significant apoptosis related GO terms, negative regulation of apoptosis, and anti-apoptosis, which overlap significantly. We found that genes annotated with these terms show decreased expression 24 hours after cardiac CTA radiation exposure (**Figure 4** and **Supplemental Table 5**), consistent with increased apoptosis. Although cell cycle and DNA repair were not significant, we observed a weak trend of increased expression of DNA repair genes and decreased expression of cell cycle genes (**Supplemental Figure 4C**). We believe this finding is consistent with the relative timing of DNA repair and apoptosis following cardiac CTA

radiation, since complete resolution of DNA damage occurred within 2 hours post-radiation in most patients and hence was undetectable in the transcriptome data collected 24 hours after cardiac CTA.

Apoptosis by immunohistochemistry. Patients with evidence of apoptosis by flow cytometry also had expression of the protein BAX by immunohistochemistry (data not shown).

In vitro studies. Findings from *in vitro* studies provide important information about the variability and repeatability of measurements in a controlled setting. Exposure of whole blood to doses as low as 12.5 mGy resulted in significant increases in phosphorylation of H2AX (4.2±0.2% vs. 2.6±0.1%, p=0·02), p53 (6.7±0.5% vs. 4.1±0.1%, p=0·005), and ATM (8.7±2.6% vs. 2.1±0.1%, p=0.02) compared to sham control (**Supplemental Figure 6**). Samples were measured three times and were reproducible with minimal differences. The higher variability in measures after radiation exposure compared to minimal variability after sham treatment suggests that variability is due to individual differences in response to radiation rather than the limitations of measurement. These findings are consistent with findings from our in vivo studies. Real time qRT-PCR confirmed that the selected genes were up-regulated at least 1.5-fold after exposure to 5,000 mGy of radiation compared to sham controls, with the greatest change noted in GADD45A (6.3-fold), DDB2 (6.8-fold), and XPC (4.4-fold) at 24 hours post radiation. With the exception of GADD45A and CDKN1A, tested genes were significantly up-regulated after exposure to 25 mGy of radiation, albeit to a lesser degree than those treated with 5,000 mGy of radiation. At least 1.5-fold induction was noted in the following four genes 24 hours after exposure to 25 mGy of radiation compared to sham control: 1) MDM2 (1.5-fold), 2) XPC (1.7-fold), 3) DDB2 (1.6-fold), and 4) TNFRS10b

(1.6-fold). With the exception of CDKN1A and ATF6, the peak change in gene expression occurred at 24 hours post radiation. Changes in gene expression declined by 36 hours post-radiation.

SUPPLEMENTAL FIGURES AND TABLES

Supplemental Figure 1. DNA damage detected in individuals exposed to radiation stratified by dose. Scatterplot graphs of proteomic biomarkers of DNA damage in individual patients stratified by dose (n=57). Circles, triangles, and squares represent phosphorylated H2AX, p53, and ATM, respectively. For better visualization of individual patients who had similar doses, we used closed and open symbols.

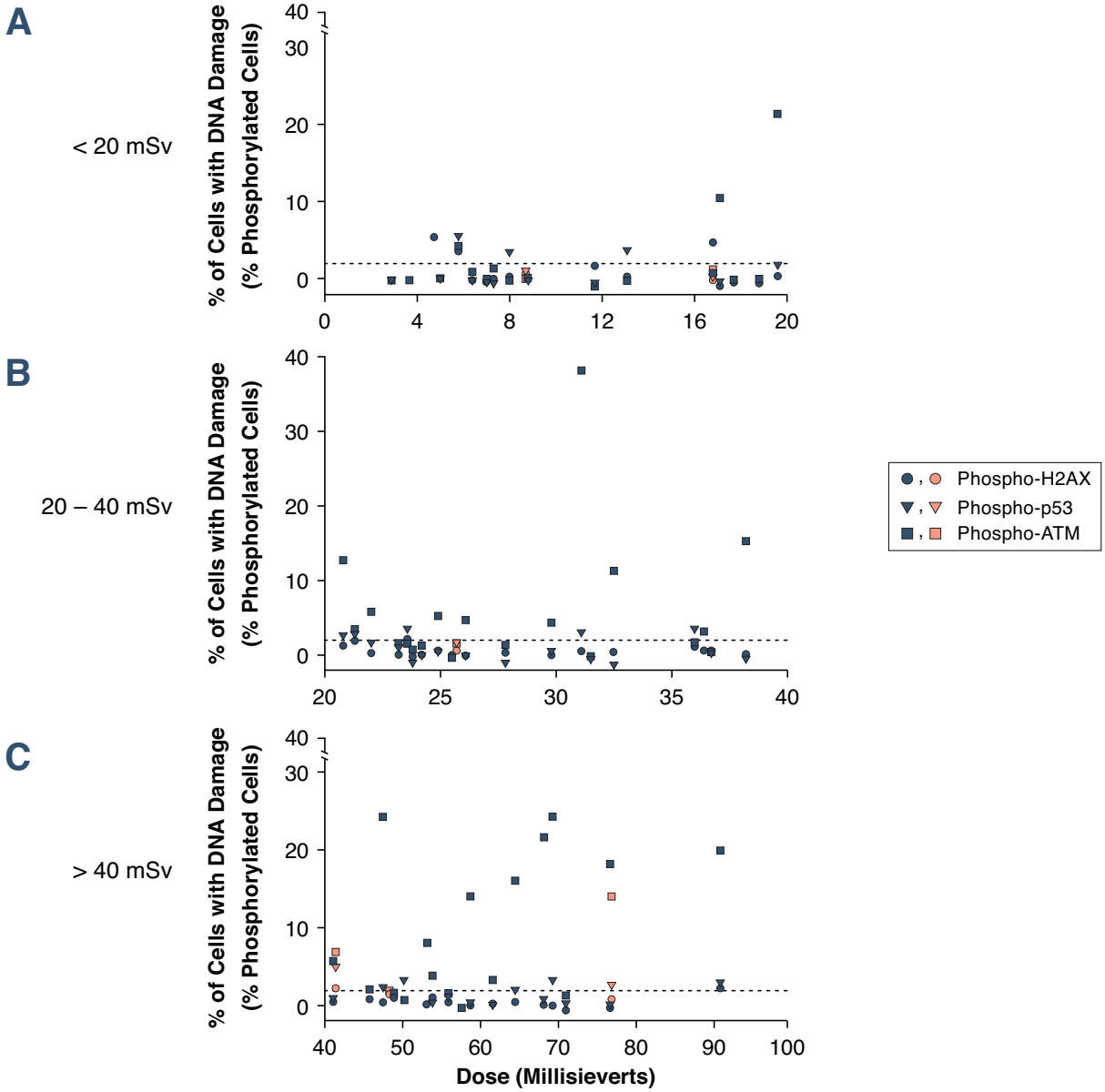

Supplemental Figure 2. Bar graphs showing the fold-difference in gene expression *in vitro* at various time points after radiation. Peak changes in gene expression are noted at 24 hours post radiation.

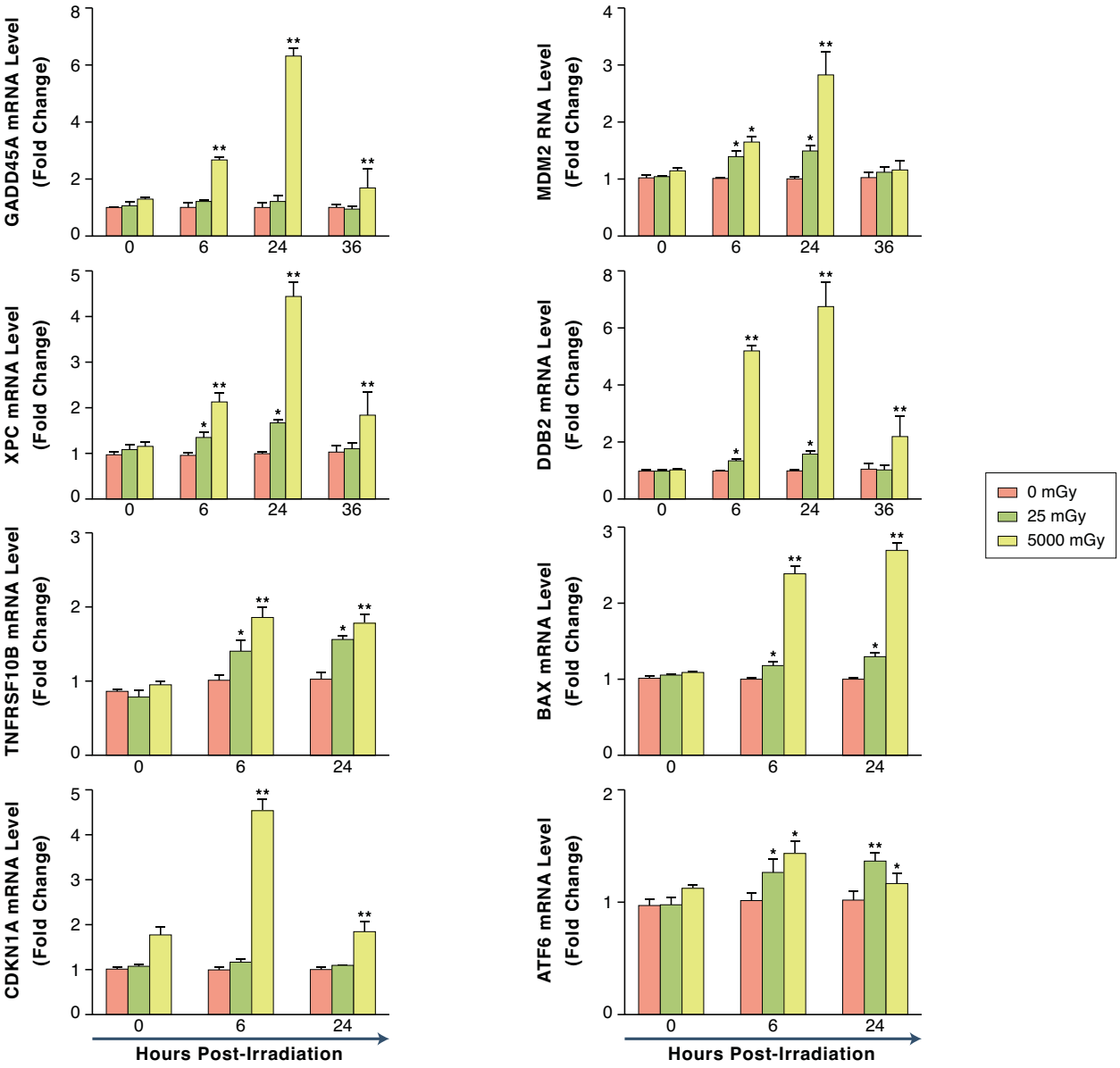

Supplemental Figure 3. Change in apoptosis over time detected in individuals exposed to low-dose radiation. **(A-C)** Line graphs of the change in apoptosis detected over time using flow cytometry stratified by dose (n=25). Median apoptosis is shown in the graph insert. (**D**) Scatterplot graph of the correlation analysis between the degree of apoptosis and radiation dose (n=25).

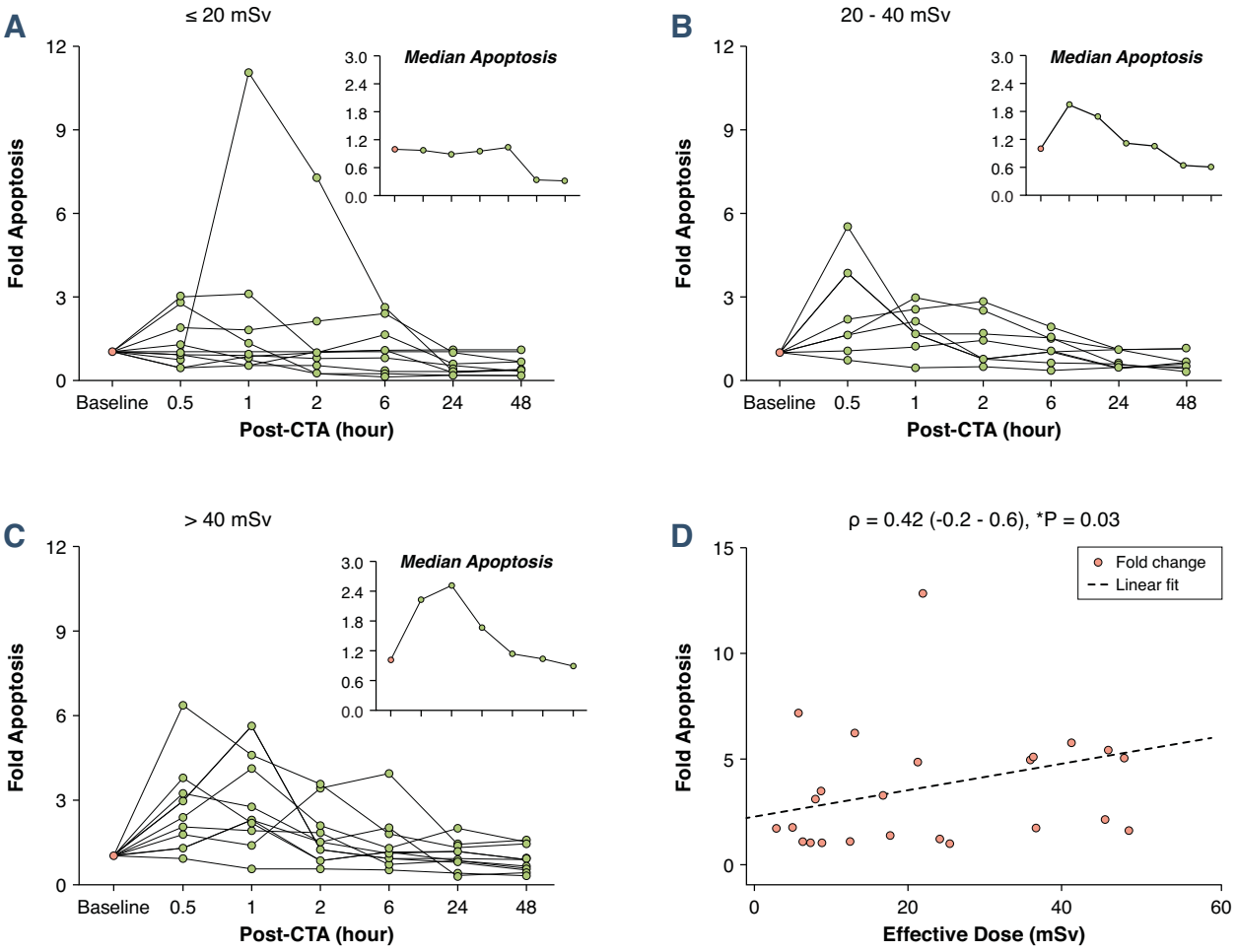

Supplemental Figure 4. Changes in the whole genome detected after low-dose radiation exposure. **(A)** Clustering of the 6 samples using the transcriptome data. The transcriptome data are obtained through RNA-sequencing of 3 selected individuals before and 24 hours after cardiac CTA. Each row corresponds to one gene. Darkness of the color maps to the log2 transformed expression levels of the genes in the 6 samples. Complete linkage hierarchical clustering of the genes was performed based on Euclidian distance. **(B)** The transcriptional regulatory network among active transcription factors obtained by linear model (see **Supplemental Methods** section for details). Each node represents a transcription factor that is significant at q-value 0.05. Edge color represents the average target gene expression changes. Red/green, target genes are on average higher/lower expressed after cardiac CTA exposure. **(C)** QQ plots showing the associations of cell cycle and DNA repair GO terms (A) and Reactome pathways (B) with transcriptional responses to cardiac CTA exposure. These gene sets are not significant after multiple test correction. The transcriptome data are obtained through RNA-sequencing of 3 selected individuals before and 24 hours after cardiac CTA.

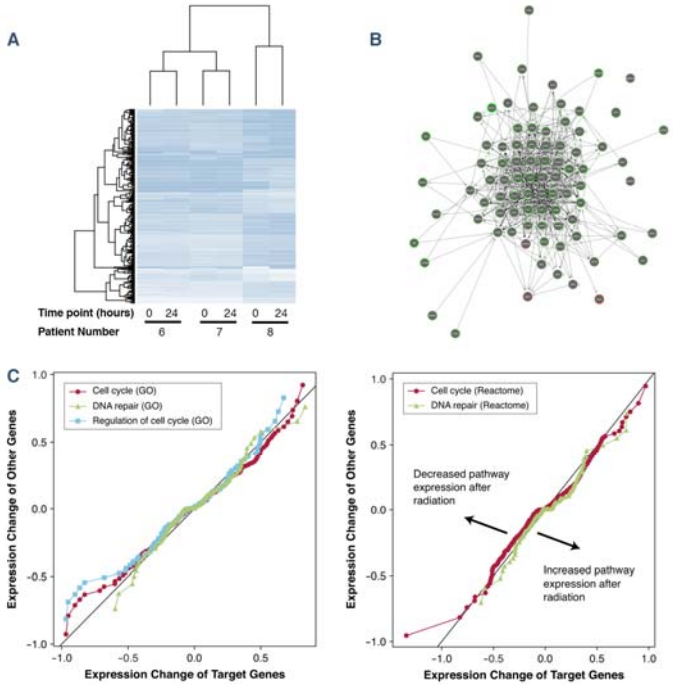

Supplemental Figure 5. Changes in the expression of individual genes involved in repair and apoptosis over time. Line graphs of the change in gene expression of **(A)** *DDB2*, **(B)** *XRCC4*, and **(C)** *BAX* over time in individual patients. Median change in gene expression at each time point is shown by the horizontal bar overlaid over each time point. *Statistically significant at p<0.01.

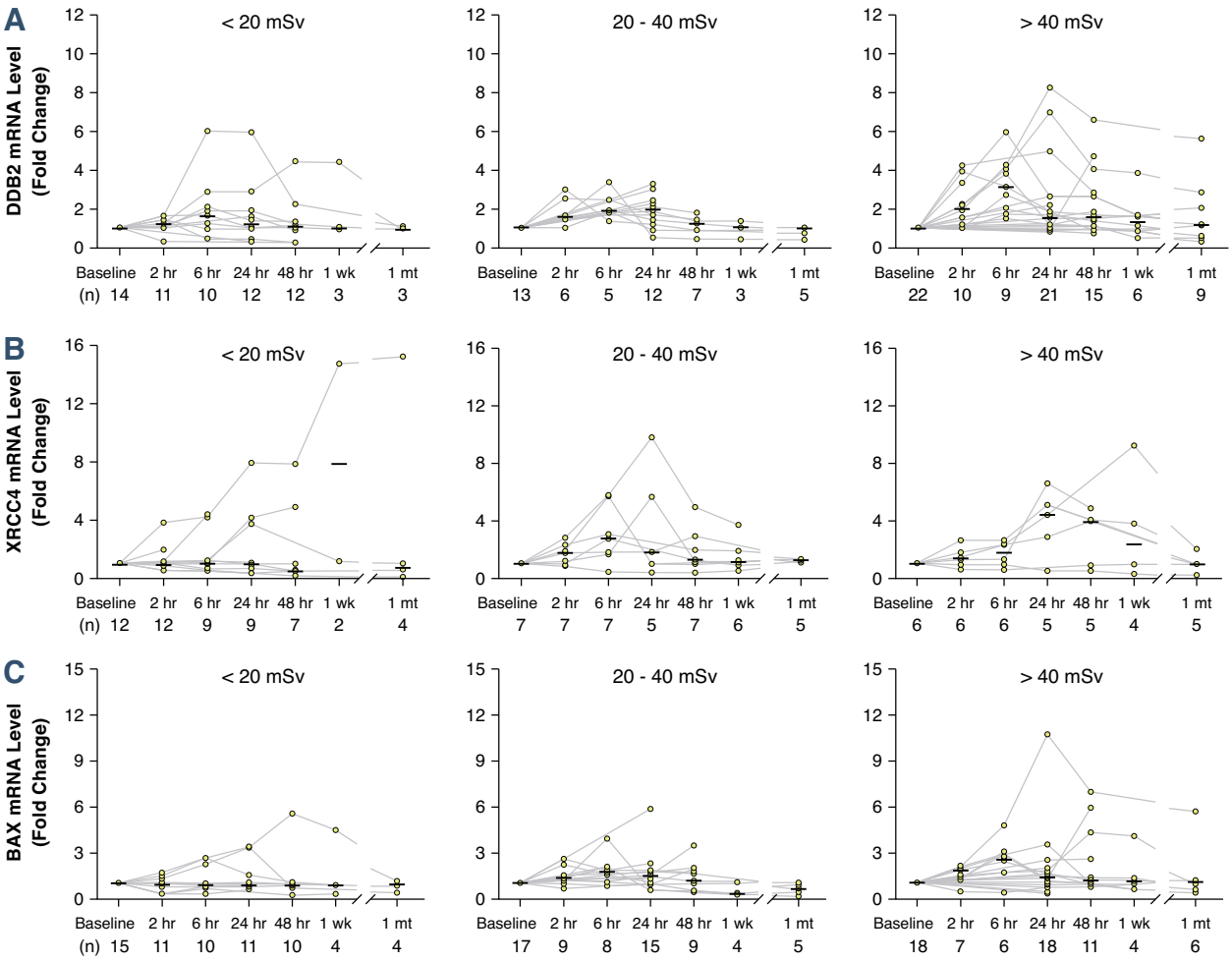

Supplemental Figure 6. Increased radiation-induced H2AX, p53, and ATM in T lymphocytes *in vitro.* FACS analysis of $CD3^+$ T lymphocyte populations using co-staining with H2AX and γH2AX reveals accumulation of γH2AX in irradiated cells compared to control. Bar graph shows the percentages of phosphorylated proteins detected by FACS analysis compared to baseline (n=10,000 cells per group): **(A)** H2AX, **(B)** p53, and **(C)** ATM.

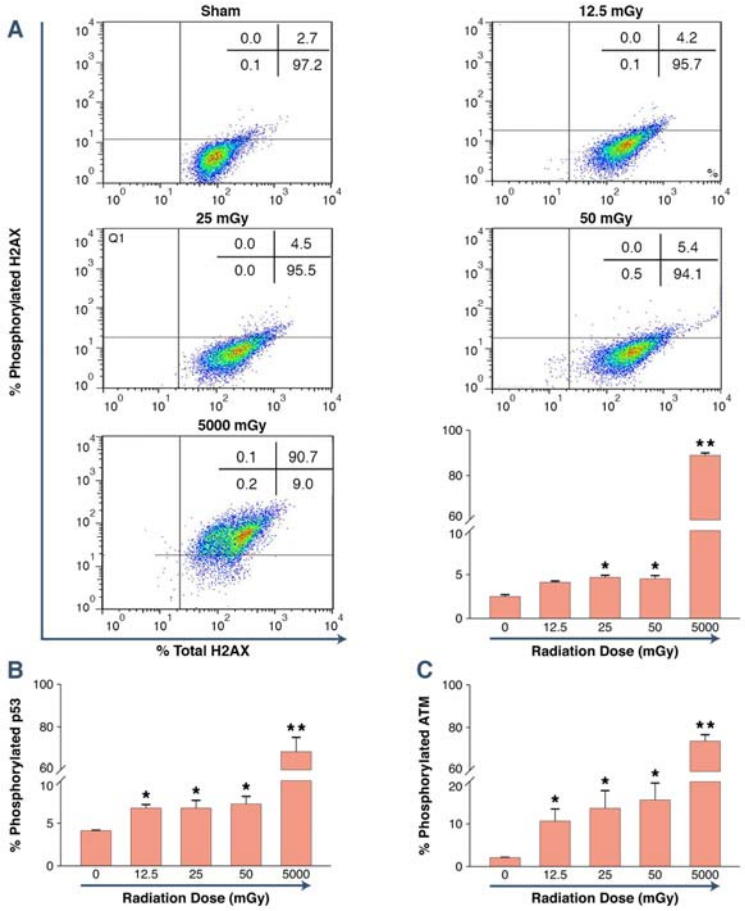

Supplemental Table 1. Selected genes involved in DNA repair and apoptosis.

Gene Symbol (OMIM No.)	Description	Function
ATF6 (605537)	Activating transcription factor 6	Apoptosis
BAX (600040)	Bcl-2-associated X protein	Apoptosis
BBC3 (60584)	BCL2 binding component 3	Apoptosis
C12ORF5 (610775)	Chromosome 12 open reading frame 5	Cell cycle
CCNG1 (601578)	Cyclin G1	Cell cycle
CDK4 (123829)	Cyclin-dependent kinase 4	Cell cycle
CDKN1A (611420)	Cyclin-dependent kinase inhibitor 1A	Cell cycle
CRADD (603454)	CASP2 and RIPK1 domain containing adaptor with death domain	Apoptosis
DCLRE1C (605988)	DNA cross-link repair 1C	DNA repair
DDB2 (60811)	Damage-specific DNA binding protein 2	DNA repair and Apoptosis
EXO1 (606063)	Exonuclease 1	DNA repair
FDXR (13270)	Ferredoxin reductase	Apoptosis
GADD45A (126355)	Growth arrest and DNA-damage-inducible, alpha	Cell cycle
JUN (16560)	Jun proto-oncogene	Cell cycle
MAP4K4 (176949)	Mitogen-activated protein kinase kinase kinase kinase 4	Apoptosis
MDM2 (164785)	Mdm2 p53 binding protein homolog	Cell cycle
PCNA (176740)	Proliferating cell nuclear antigen	DNA repair
PEG3 (601483)	Paternally expressed 3	Apoptosis
POLH (603968)	Polymerase (DNA directed), eta	DNA repair
RAD50 (604040)	RAD 50 homolog	DNA repair
RAET1E (609243)	Retinoic acid early transcript 1E	Apoptosis
SESN1 (606103)	Sestrin 1	Cell cycle
SH3RF1 (613377)	SH3 domain containing ring finger 1	Apoptosis
TP53 (611153)	Tumor protein p53	Apoptosis
XPA (611153)	Xeroderma pigmentosum, complementation group A	DNA repair
XPC (191170)	Xeroderma pigmentosum, complementation group C	DNA repair
XRCC4 (194363)	X-ray repair complementing defective repair in Chinese hamster cells 4	DNA repair

Supplemental Table 2. Standard protocols for cardiac computed tomographic angiography.

Category: Aorta (n=30, 42%)

	Chest Non Con Helical	Pre-Monitoring Axial	Monitoring Axial	Gated Chest Helical
Tube voltage (kV)	120	120	120	120
Rotation time (s)	0.5	0.33	0.33	0.33
Spiral pitch	0.8	N/A	N/A	0.2
Collimation (mm)	24 x 1.2	1 x 10	1 x 10	64 x 0.6

Category: Coronary (n=23, 32%)

	Ca-Score Axial	Pre-Monitoring Axial	Monitoring Axial	Coronary CTA Helical
Tube voltage (kV)	120	120	120	120
Rotation time (s)	0.26	0.33	0.33	0.33
Spiral pitch	N/A	N/A	N/A	0.2
Collimation (mm)	24 x 1.2	1 x 10	1 x 10	64 x 0.6

Category: Valve replacement (n=18, 25%)

	C/A/P Non Con Helical	Pre-Monitoring Axial	Monitoring Axial	DS_ChestPain Helical	Body Angio Helical
Tube voltage (kV)	120	120	120	120	120
Rotation time (s)	0.5	0.33	0.33	0.33	0.33
Spiral pitch	0.8	N/A	N/A	0.2	0.8
Collimation (mm)	24 x 1.2	1 x 10	1 x 10	64 x 0.6	64 x 0.6

Category: Left atrial mapping (n= 3, 4%)

	Axial	Cardiac Helical
Tube voltage (kV)	120	120
Rotation time (s)	0.35	0.35
Spiral pitch	N/A	0.2
Collimation (mm)	1 x 5	64 x 0.625

Supplemental Table 3. Summary statistics of the disappearance of proteomic biomarkers over time.

		Time after radiation exposure (minutes)									
		Early (minutes)					Late (hours)				
Biomarker	**Background**	**5**	**15**	**30**	**60**	**120**	**6**	**24**	**48**	**189**	**384**
γ H2AX (*n=10)											
Mean	0.02	0.06	0.06	0.12	0.06	0.04	0.02	0	0	0	0
Median	0	0	0.05	0.1	0.01	0	0	0	0	0	0
Minimum	0	0	0	0	0	0	0	0	0	0	0
Maximum	0.2	0.43	0.18	0.45	0.2	0.15	0.18	0	0	0	0
53BP1 (*n=14)											
Mean	0.01	0.07	0.12	0.05	0.04	0.03	0.02	0.02	0.01	0.01	0
Median	0	0.06	0.1	0.04	0	0	0	0	0	0	0
Minimum	0	0	0	0	0	0	0	0	0	0	0
Maximum	0.1	0.2	0.25	0.19	0.18	0.15	0.1	0.1	0.08	0.08	0
ATM (*n=14)											
Mean	0.02	0.09	0.14	0.18	0.06	0.08	0.06	0.04	0.04	0.01	0
Median	0	0.05	0.1	0.13	0.05	0.03	0	0	0	0	0
Minimum	0	0	0	0	0	0	0	0	0	0	0
Maximum	0.1	0.33	0.33	0.83	0.15	0.58	0.53	0.53	0.53	0.08	0.05

* Number of patients with evaluable samples.

Supplemental Table 4. Demographics and clinical characteristics of patient samples sent for whole genome profiling.

Patient ID	Age (yrs)	Sex	BMI kg/m^2	Race	Smoking	Cancer History	Type of Study	Dose (mSv)	Contrast (g of iodine)
6	81	F	26.2	Caucasian	Never	No	Aorta	21.3	33.3
7	59	F	21.1	Caucasian	Never	No	Aorta	48.8	33.3
8	77	M	30.4	Caucasian	Former	No	Valve	36.0	30.0

Supplemental Table 5. Selected gene annotations associated with transcriptional response of human T lymphocytes to low-dose radiation from cardiac CTA.

Annotation	Fisher's Exact Test		Wald t-test		Source
	OR#	p-value	T	p-value	
Negative regulation of apoptosis	2.9	8.3E-3	-4.4	9.3E-6***	GO
Cellular biosynthetic process	4.4	3.6E-5**	-6.4	5.3E-10***	GO
AP1 pathway	19.8	1.5E-6**	-6.6	3.9E-11***	PID
Myc pathway	2.7	1.9E-4**	-4.6	3.6E-6***	PID
Pentose phosphate pathway (Erythrocyte)	60.2	1.0E-3*	-4.2	2.3E-5**	PharmGKB
HIF1 pathway	6.4	1.4E-3*	-4.4	1.2E-5***	PID
NFAT pathway	18.7	2.0E-3*	-4.2	2.9E-5**	PID
cMyb pathway	2.5	1.1E-2	-3.9	9.2E-5**	PID
HIF2A (EPAS1)	3.2	4.9E-06***	-4.4	1.0E-05***	TFTG
NFKB1	2.2	1.3E-04**	-3.8	1.2E-04***	TFTG
NFATC1	3.5	8.2E-04**	-7.6	4.2E-14***	TFTG
GLIS1	0.9	1.0E-03**	4.0	5.4E-05***	TFTG
Cyclin T2 (CCNT2)	1.6	1.3E-03**	-4.0	7.4E-05***	TFTG
TP53	3.5	4.2E-03*	-3.0	3.1E-03**	TFTG
HIF1A	1.7	1.5E-01	-2.9	3.3E-03**	TFTG

Full association result is provided in Supplemental Tables 7-9. * p-values that are significant after multiple-test correction; * q-value < 0.1; ** q-value < 0.05; *** q-value < 0.001. #OR, odds ratios for the enrichment in gene annotations in top 5% most differentially expressed genes that have decreased expression upon CT radiation exposure. GO, Gene Ontology database, http://www.ebi.ac.uk/QuickGO; PID, Pathway Interaction Database, http://pid.nci.nih.gov; PharmGKB, the Pharmacogenomics Knowledgebase, http://pharmgkb.org. TFTG, in house compiled transcription factor target gene database.

Supplemental Table 6. Gene ontology biological process annotations significantly associated with radiation response.

Functional Annotation	Fisher's Exact Test				Linear Model Wald Test		
	p-value	q-value	upper-tail OR[#]	lower-tail OR[#]	p-value	q-value	T
Cellular biosynthetic process*	3.6E-05	2.7E-02	0.7	4.4	2.0E-10	1.2E-07	-6.4
Translation	9.9E-05	2.7E-02	0.0	6.6	5.3E-10	1.6E-07	-6.2
Immune system process	7.7E-05	2.7E-02	0.7	3.3	7.6E-04	1.3E-02	-3.4
Regulation of metabolic process	2.2E-04	3.7E-02	0.5	2.8	3.9E-06	2.4E-04	-4.6
Regulation of cellular Metabolic process	1.8E-04	3.7E-02	0.5	2.9	4.6E-06	2.6E-04	-4.6
Cytokine production	4.6E-04	5.2E-02	0.0	5.8	1.1E-05	5.1E-04	-4.4
Regulation of gene expression	5.2E-04	5.2E-02	0.6	2.6	6.3E-05	1.8E-03	-4.0
Regulation of RNA metabolic process	3.8E-04	5.2E-02	0.5	2.4	2.6E-04	5.2E-03	-3.7
Regulation of transcription DNA dependent	5.7E-04	5.2E-02	0.5	2.4	4.5E-04	8.7E-03	-3.5
Transcription DNA dependent	8.3E-04	6.5E-02	0.3	2.1	2.7E-05	9.8E-04	-4.2
RNA biosynthetic process	8.6E-04	6.5E-02	0.3	2.1	3.0E-05	9.8E-04	-4.2
transcription	1.1E-03	7.5E-02	0.6	2.1	2.8E-05	9.8E-04	-4.2
Negative regulation of biological process	1.2E-03	7.5E-02	0.6	3.7	6.0E-05	1.8E-03	-4.0
Negative regulation of cellular process	1.4E-03	8.0E-02	0.7	3.9	4.2E-05	1.3E-03	-4.1
Regulation of nucleobase, -side, -tide and nucleic acid Metabolic process	2.0E-03	1.0E-01	0.7	2.1	8.2E-04	1.3E-02	-3.3
Regulation of transcription	2.1E-03	1.0E-01	0.8	2.3	1.2E-03	1.7E-02	-3.2
Regulation of cytokine production	2.0E-03	1.0E-01	0.0	0.0	4.9E-03	4.8E-02	-2.8

Multi-test correction is performed and q-value cutoff 0.1 is applied. OR[#]: odds ratio; LM, linear model. * The biological process (as well as negative regulation of apoptosis) are visualized in Figure 2 and Supplemental Figure 4A.

Supplemental Table 7. Signaling and metabolic pathways significantly associated with cardiac CTA radiation response.

Functional Annotation	Fisher's Exact Test				Linear Model Wald Test		
	p-value	q-value	upper-tail OR[#]	lower-tail OR[#]	p-value	q-value	T
PID: AP1 PATHWAY*	1.5E-06	2.3E-03	0	19.8	3.9E-11	2.4E-08	-6.6
BIOCARTA: IL5 PATHWAY	8.6E-06	6.6E-03	0	79.1	6.5E-09	8.8E-07	-5.8
REACTOME: PEPTIDE CHAIN ELONGATION	2.3E-05	1.2E-02	0	7.3	4.9E-10	1.5E-07	-6.2
MIPS: RIBOSOME CYTOPLASMIC	6.4E-05	2.5E-02	0	3.8	3.6E-09	5.4E-07	-5.9
REACTOME: 3' UTR MEDIATED TRANSLATIONAL REGULATION	9.9E-05	3.1E-02	0	2.7	2.5E-09	4.9E-07	-6.0
KEGG: LEISHMANIA INFECTION	1.2E-04	3.1E-02	3.2	9.5	6.2E-06	3.3E-04	-4.5
PID: MYC ACTIVPATHWAY*	1.9E-04	4.2E-02	0	2.7	3.6E-06	2.3E-04	-4.6
KEGG: RIBOSOME	2.3E-04	4.4E-02	0	3.3	1.3E-09	3.2E-07	-6.1
KEGG: OLFACTORY TRANSDUCTION	2.8E-04	4.8E-02	0	0	4.1E-06	2.5E-04	4.6
BIOCARTA: IL3 PATHWAY	3.9E-04	6.0E-02	0	36.5	2.5E-03	3.7E-02	-3.0
REACTOME: TRANSLATION	4.7E-04	6.6E-02	0	3.6	3.8E-12	4.6E-09	-6.9
BIOCARTA: AHSP PATHWAY	6.2E-04	6.9E-02	0	61.6	3.6E-08	4.3E-06	-5.5
BIOCARTA: NKT PATHWAY	6.3E-04	6.9E-02	0	22.2	9.8E-05	3.0E-03	-3.9
REACTOME: SRP DEPENDENT COTRANSLATIONAL PROTEIN TARGETING TO MEMBRANE	7.2E-04	6.9E-02	0	2.5	8.5E-11	3.4E-08	-6.5
PharmGKB: PA165971634 Pentose Phosphate Pathway (Erythrocyte)*	1.0E-03	7.5E-02	0	60.2	2.3E-05	1.0E-03	-4.2
MIPS: 60S RIBOSOMAL SUBUNIT CYTOPLASMIC	1.1E-03	7.5E-02	0	6.5	5.2E-08	5.7E-06	-5.4
PID: PDGFRAPATHWAY	1.1E-03	7.5E-02	0	12.1	1.9E-03	3.2E-02	-3.1
REACTOME: INFLUENZA VIRAL RNA TRANSCRIPTION AND REPLICATION	1.1E-03	7.5E-02	0	2.7	1.0E-07	1.0E-05	-5.3
PID: HIF1 TFPATHWAY*	1.4E-03	7.9E-02	3.3	6.4	1.2E-05	6.0E-04	-4.4
PID: IL12 2PATHWAY	1.6E-03	7.9E-02	0	6.4	1.2E-04	3.6E-03	-3.8
KEGG: ALLOGRAFT REJECTION	1.8E-03	7.9E-02	0	5.5	4.6E-05	1.6E-03	-4.1
PID: TCRCALCIUMPATHWAY	1.9E-03	7.9E-02	0	23.1	5.0E-06	2.7E-04	-4.6
REACTOME: OLFACTORY SIGNALING PATHWAY	1.9E-03	7.9E-02	0	0	4.4E-06	2.5E-04	4.6
PID: NFAT TFPATHWAY*	2.0E-03	7.9E-02	4.5	18.7	2.9E-05	1.1E-03	-4.2
REACTOME: PIP3 ACTIVATES AKT SIGNALING	2.0E-03	7.9E-02	0	0	2.2E-03	3.4E-02	-3.1
REACTOME: NONSENSE MEDIATED DECAY ENHANCED BY THE EXON JUNCTION COMPLEX	2.2E-03	7.9E-02	0	2.6	1.1E-05	5.6E-04	-4.4
PID: PRLSIGNALINGEVENTSPATHWAY	2.3E-03	7.9E-02	0	10.6	1.4E-03	2.8E-02	-3.2
KEGG: ASTHMA	2.3E-03	7.9E-02	0	15.2	2.1E-05	9.3E-04	-4.3
PID: IL6 7PATHWAY	2.6E-03	8.6E-02	4.5	13.5	1.7E-03	3.0E-02	-3.1
KEGG: AUTOIMMUNE THYROID DISEASE	2.7E-03	8.8E-02	0	3.8	2.1E-03	3.4E-02	-3.1
REACTOME: METABOLISM OF mRNA	2.9E-03	8.9E-02	0	1.2	3.0E-05	1.1E-03	-4.2
BIOCARTA: DREAM PATHWAY	3.0E-03	9.0E-02	0	15.1	1.4E-03	2.7E-02	-3.2
BIOCARTA: ARENRF2 PATHWAY	3.0E-03	9.0E-02	0	20.1	1.4E-04	4.0E-03	-3.8

Multi-test correction is performed and q-value cutoff 0.1 is applied. OR[#]: odds ratio; LM, linear model. * These pathways are visualized in Figure 2 and Supplemental Figure 4A.

Supplemental Table 8. Transcription factors with significantly altered activities according to their target gene expression pattern

Transcription Factor (OMIM No)	Annotation[&]	Fisher's Exact Test				Linear Model Wald Test		
		p-value	q-value	upper-tail OR[#]	lower-tail OR[#]	p-value	q-value	T
SMARCA4 (603254)	Chromatin remodeling	3.8E-06	6.2E-04	1.8	13.6	4.3E-11	2.0E-09	-6.6
EPAS1*, HIF2-alpha (603349)	Stress response	4.9E-06	6.2E-04	0	6.4	1.0E-05	9.7E-05	-4.4
MYB (189990)	Cell cycle	2.4E-05	2.3E-03	0	4.0	1.7E-08	3.0E-07	-5.6
NFKB1* (164011)	Apoptosis, Stress response	1.3E-04	8.1E-03	1.4	2.8	1.2E-04	7.2E-04	-3.8
TALI (187040)	Cell growth and differentiation	8.6E-05	6.5E-03	0.6	1.6	2.4E-13	2.8E-11	-7.3
SREBF1 (184756)	Stress response	1.6E-04	8.5E-03	1.9	5.5	4.3E-01	4.3E-01	-0.8
TBP (60075)	Cell proliferation	2.2E-04	1.0E-02	0	6.3	1.0E-08	2.1E-07	-5.7
BACH2 (605394)	Cell cycle	2.9E-04	1.2E-02	0.6	1.5	3.6E-08	6.0E-07	-5.5
CBFB (121360)	Cell cycle	5.0E-04	1.9E-02	0.6	1.3	5.8E-10	1.9E-08	-6.2
KAT2A* (602301)	Cell cycle, Apoptosis	6.6E-04	2.3E-02	0	34.7	5.5E-06	5.6E-05	-4.5
NFATC1* (600489)	Transcription regulator	8.2E-04	2.4E-02	0	7.2	4.2E-14	9.9E-12	-7.6
SP1 (189906)	Transcription regulator	9.5E-04	2.4E-02	0.9	2.4	2.7E-07	3.5E-06	-5.1
GLIS1* (610378)	Transcription regulator	1.0E-03	2.4E-02	1.8	0	5.4E-05	3.8E-04	4.0
KLF4 (602253)	Transcription regulator	1.0E-03	2.4E-02	0	60.2	5.5E-04	2.8E-03	-3.5
GFI1 (600871)	Cell cycle	1.0E-03	2.4E-02	0	0	1.4E-01	1.9E-01	-1.5
CCNT2* (603862)	Cell cycle	1.3E-03	2.8E-02	0	3.1	7.4E-05	5.1E-04	-4.0
POU2F2 (164176)	Immune response	1.3E-03	2.8E-02	2.4	15.3	7.6E-05	5.1E-04	-4.0
FOXM1 (602341)	Immune response	1.5E-03	3.0E-02	0	0.7	3.4E-05	2.6E-04	-4.1
DLX1 (60029)	Transcription regulator	1.6E-03	3.0E-02	0.7	1.7	1.1E-05	9.7E-05	-4.4
SPI1 (165170)	Hematopoiesis	1.8E-03	3.2E-02	0.8	1.4	1.7E-11	9.9E-10	-6.7
ETS1 (164720)	Immune response, Hematopoiesis	2.1E-03	3.7E-02	0.7	2.8	4.6E-03	1.6E-02	-2.8
TCF12 (600480)	Immune response	2.2E-03	3.7E-02	0.5	1.5	6.2E-11	2.4E-09	-6.5

Multi-test correction is performed and q-value cutoff 0.1 is applied to select active transcription factors. OR[#]: odds ratio; LM, linear model. * These transcription factors (as well as HIF1A) are visualized in Figure 4 and Supplemental Figure 4. & These annotations are obtained based on manual annotations of GO biological processes.

Supplemental Table 8 (continued).

Transcription Factor (OMIM No)	Annotation[&]	Fisher's Exact Test				Linear Model Wald Test		
		p-value	q-value	upper-tail OR[#]	lower-tail OR[#]	p-value	q-value	T
EBF1 (164343)	Transcription regulator	2.3E-03	3.7E-02	0.8	3.3	3.6E-03	1.3E-02	-2.9
TAF (313650)	Cell Cycle	2.6E-03	4.0E-02	0	2.2	4.7E-09	1.1E-07	-5.9
E2F1 (189971)	Cell cycle, Apoptosis	2.9E-03	4.2E-02	0.4	1.4	5.3E-07	6.6E-06	-5.0
MYC (190080)	Cell cycle	3.0E-03	4.2E-02	0.7	2.2	1.7E-09	4.3E-08	-6.0
GATA2 (137295)	Regulator of the AP1 pathway	3.2E-03	4.3E-02	0.8	1.7	8.0E-10	2.3E-08	-6.1
RUNX1 (151385)	Hematopoiesis	3.7E-03	4.8E-02	0.6	1.3	1.0E-12	7.9E-11	-7.1
TP53* (191170)	Cell cycle, Apoptosis, DNA repair, Stress response	4.2E-03	5.3E-02	0.8	6.2	3.1E-03	1.2E-02	-3.0
GFI1B (604383)	Cell cycle	5.0E-03	6.2E-02	0	0	1.5E-03	6.4E-03	-3.2
ATF1 (123803)	Stress response	5.3E-03	6.3E-02	1.3	2.4	2.0E-03	8.7E-03	-3.1
BCOR (300485)	Transcription regulator	6.0E-03	6.8E-02	1.2	1.7	2.9E-06	3.1E-05	-4.7
SMC3 (606062)	Cell cycle	6.2E-03	6.8E-02	0.6	2.8	9.2E-04	4.3E-03	-3.3
ZBTB7A (605878_)	Cell survival	6.2E-03	6.8E-02	0	2.4	1.3E-02	3.4E-02	-2.5
ERG (165080)	Cell cycle, Apoptosis	7.6E-03	7.8E-02	0.5	0.7	1.5E-08	3.0E-07	-5.7
SMARCB1 (601607)	Chromatin Remodeling	8.7E-03	8.7E-02	2.0	3.9	1.3E-04	7.3E-04	-3.8
CEBPA (116897)	Cell proliferation	9.3E-03	9.1E-02	1.0	1.4	3.9E-05	2.9E-04	-4.1
WT1 (707102)	Transcription regulator	1.0E-02	9.7E-02	0	11.1	5.1E-03	1.7E-02	-2.8

Multi-test correction is performed and q-value cutoff 0.1 is applied to select active transcription factors. OR[#]: odds ratio; LM, linear model. * These transcription factors (as well as HIF1A) are visualized in Figure 4 and Supplemental Figure 4. & These annotations are obtained based on manual annotations of GO biological processes.

Supplemental Table 9. Summary of RNA-seq differential expressions for the genes that are evaluated by qPCR.

Gene Symbol	log2(fold change)	Wald t	p-value
BAX*	0.56	10.6	0.009
BBC3	0.38	1.9	0.202
CCNG1	0.25	1.6	0.243
CDK4	-0.13	-0.6	0.633
CDKN1A	-0.51	-2.0	0.185
CRADD	1.13	3.3	0.082
DDB2*	0.35	1.3	0.312
EXO1	0.50	0.9	0.480
FDXR	0.82	6.9	0.020
GADD45A	0.11	0.3	0.792
JUN	-0.49	-1.2	0.352
PCNA	-0.11	-0.5	0.676
POLH	-0.10	-2.0	0.186
RAD50	0.78	5.7	0.030
RAET1E	0.88	1.4	0.300
SESN1	0.63	2.0	0.180
SH3RF1	1.22	1.8	0.219
TP53*	-0.29	-3.1	0.091
XPA	0.33	1.6	0.244
XPC	-0.22	-0.7	0.550
XRCC4*	0.32	0.7	0.551

The Wald t statistics and p-values are obtained by the linear model described in the method section.

Supplemental Table 10: Results of repeated measures of ANOVA for significant genes.

Gene	Source	Partial Sum of Squares	df	Mean Square	F	R^2	p-value*
DDB2	Time	167262	6	27877	15.8	0.50	<0.0001
	Residual	261812	148	1769			
XRCC4	Time	16659	6	2776	3.54	0.51	0.01
	Residual	83235	106	785			
BAX	Time	20577	6	3429	2.50	0.45	0.04
	Residual	167659	122	1374			

* Adjusted by Huynh-Feldt epsilon

Supplemental Table 11: Summary of RNA-seq differential expressions for the individual genes (please see excel spreadsheet).

SUPPLEMENTAL REFERENCES

1. International Commission on Radiological Protection. *Basic anatomical and physiologic data for use in radiological protection: Reference value - report of age-gender-related differences in the anatomaical and physiological chracteristics of reference individuals.* ICRP Publication 89.2002;32(3-4):1-277.
2. Bolstad BM, Irizarry RA, Astrand M, Speed TP. A comparison of normalization methods for high density oligonucleotide array data based on variance and bias. *Bioinformatics.* 2003;19(2):185-193.
3. Gerstein MB, Kundaje A, Hariharan M, et al. Architecture of the human regulatory network derived from encode data. *Nature.* 2012;489(7414):91-100.
4. Ashburner M, Ball CA, Blake JA, et al. Gene ontology: Tool for the unification of biology. The gene ontology consortium. *Nat Genet.* 2000;25(1):25-29.
5. Joshi-Tope G, Gillespie M, Vastrik I, et al. Reactome: A knowledgebase of biological pathways. *Nucleic Acids Res.* 2005;33(Database issue):D428-432.
6. Kanehisa M, Goto S. Kegg: Kyoto encyclopedia of genes and genomes. *Nucleic Acids Res.* 2000;28(1):27-30.
7. Nishimura D. Biocarta - http://www.Biocarta.Com. . *Biotech Software & Internet Report.* 2001;2(3):117-120.
8. Hewett M, Oliver DE, Rubin DL, et al. Pharmgkb: The pharmacogenetics knowledge base. *Nucleic Acids Res.* 2002;30(1):163-165.
9. Mehta C, Patel N. A network algorithm for performing fisher's exact test in r × c contingency tables. *Journal of the American Statistical Association.* 1983;78(382):427-434.
10. Sekhon R, Briskine R, Hirsch C, et al. Maize gene atlas developed by rna sequencing and comparative evaluation of transcriptomes based on rna sequencing and microarrays. *PLoS One.* 2013;8(4):e61005.
11. Storey JD. The positive false discovery rate: A bayesian interpretation and the q-value. *The Annals of Statistics.* 2003;31(6):2013-2035.
12. Wang CY, Mayo MW, Baldwin AS, Jr. Tnf- and cancer therapy-induced apoptosis: Potentiation by inhibition of nf-kappab. *Science.* 1996;274(5288):784-787.
13. Bertout JA, Majmundar AJ, Gordan JD, et al. Hif2alpha inhibition promotes p53 pathway activity, tumor cell death, and radiation responses. *Proc Natl Acad Sci U S A.* 2009;106(34):14391-14396.
14. Riganti C, Gazzano E, Polimeni M, Aldieri E, Ghigo D. The pentose phosphate pathway: An antioxidant defense and a crossroad in tumor cell fate. *Free Radic Biol Med.* 2012;53(3):421-436.
15. Tuttle S, Stamato T, Perez ML, Biaglow J. Glucose-6-phosphate dehydrogenase and the oxidative pentose phosphate cycle protect cells against apoptosis induced by low doses of ionizing radiation. *Radiat Res.* 2000;153(6):781-787.